IOP Conference Series: Materials Science and Engineering

Influence of Discretization of Permeability Term and Mesh Size on the Prediction of Channel Segregations

To cite this article: A Kumar *et al* 2012 *IOP Conf. Ser.: Mater. Sci. Eng.* **27** 012039

View the article online for updates and enhancements.

Related content

- Effect of discretization of permeability term and mesh size on macro- and meso-segregation predictions
  Arvind Kumar, Bernard Dussoubs, Miha Založnik et al.
- Three-dimensional study of macro- and mesosegregation formation in a rectangular cavity cooled from one vertical side
  V F De Felice, K O Tveito, M Založnik et al.
- A numerical simulation of columnar solidification: influence of inertia on channel segregation
  Arvind Kumar, Miha Založnik, Hervé Combeau et al.

Recent citations

- A numerical simulation of columnar solidification: influence of inertia on channel segregation
  Arvind Kumar *et al*

This content was downloaded from IP address 193.48.49.224 on 15/02/2018 at 17:01

Influence of Discretization of Permeability Term and Mesh Size on the Prediction of Channel Segregations

A Kumar, B Dussoubs, M Založnik and H Combeau
Institut Jean Lamour, Département SI2M, CNRS – Nancy-Université – UPV-Metz, Ecole des Mines de Nancy, Parc de Saurupt CS 14234, F-54042 Nancy cedex, France

E-mail: herve.combeau@ijl.nancy-universite.fr

Abstract. Macro- and meso-segregations correspond to compositional heterogeneities at the scale of a casting. They develop during the solidification process. One of the parameters that have an essential effect on these segregations is the mush permeability, which is highly nonlinear, and varies over a wide range of magnitudes. We present simulation results for solidification of a Sn-Pb alloy in a two-dimensional cavity, highlighting the role of (i) the numerical interpolation schemes used for the finite-volume discretization of the highly-nonlinear permeability term and (ii) of the mesh size on the prediction of mesosegregations and macrosegregation. We observe that solute-rich liquid flowing through the mushy zone due to thermo-solutal convection results in patches of thin channel structures, which develop into mesosegregations. We notice little sensitivity of the predicted macrosegregation to different discretization schemes for the permeability term. However, we found their influence on the prediction of channel segregates to be significant when using coarse computational grids, customary in the simulation of industrial castings. Mesh refinement is crucial for capturing the complex phenomena in the formation of channel segregates. With a very fine mesh channels have been captured with more than one grid point along their width, allowing the determination of their width.

1. Introduction

Fluid flow in a columnar mushy zone plays an important role in the formation of macrosegregation in castings by redistributing the segregated solute elements [1, 2]. In some cases the flow triggers the formation of *channel-type mesosegregations* (also called *channel segregates*) in the mushy zone [2–5]. The interdendritic flow in the mushy region leads to perturbations of the growing columnar structure, causing instability of the growth front, which leads to further instability of the segregation map, leading to the formation of channel segregates. The formation of channel segregates in castings represents a severe form of segregation since the composition and the crystalline structure of the solid that ultimately forms within the channels differ significantly from those of the nearby solid regions.

Macrosegregation in castings was widely studied using multiscale models consisting of macroscopic models based on mixture theory [1] or volume averaging [6], coupled to models of microsegregation. In these models, the mushy zone is considered as a saturated porous medium with varying permeability, and the hydrodynamic resistance is described by a Darcy force. One of the parameters that have the largest effect on the macrosegregation is the mush permeability. The Carman-Kozeny model is widely used to calculate the permeability. For this simplest model the permeability is a function of the liquid fraction and of the dendritic arm spacing (DAS). The dependence of permeability on liquid fraction is highly nonlinear, thus a small variation in the liquid fraction can result in large variation of permeability which can significantly affect the flow in the mushy zone and hence the segregation pattern. The solution procedures of these macroscopic models involve the discretization of the macro-

Published under licence by IOP Publishing Ltd

scopic conservation equations based most often either on a finite volume formulation [1–6], or on a finite element formulation. In the finite volume formulation the discretization of the momentum balance equation requires an estimation of the volume integral of the Darcy term over the control volume (CV) by applying some discretization scheme. The way this integration is approximated to get the discretized form of the Darcy term can play an important role in the numerical predictions [4, 7]. When using staggered pressure-velocity grids, the permeability K, a function of the liquid fraction g_l, is known in the pressure CV points. The Darcy term has to be integrated over the velocity CV using an interpolation of the permeability from the adjacent pressure CVs. The objective of the present article is to investigate the effect of schemes for the discretization of the permeability term on predictions of macrosegregation and channel segregates.

2. Mathematical modeling

The conservation equations for mass, heat, solute, and momentum are averaged over both liquid and solid phase (assuming a fixed solid phase; equal and constant solid and liquid densities, except in the buoyancy term, where Boussinesq approximation is used; and Scheil law for microsegregation) [2,4].

Mass conservation:
$$\nabla \cdot \mathbf{v} = \nabla \cdot \left(g_l \mathbf{v}_l \right) = 0 \tag{1}$$

Energy conservation:
$$\rho_0 \frac{\partial h}{\partial t} + \rho_0 c_p \mathbf{v} \cdot \nabla T = \nabla \cdot \left(k \nabla T \right) \tag{2}$$

where the average enthalpy is:
$$h = g_s h_s + \left(1 - g_s\right) h_l = c_p \left(T - T_0\right) + \left(1 - g_s\right) L \tag{3}$$

Solute conservation:
$$\frac{\partial C}{\partial t} + \mathbf{v} \cdot \nabla C_l = 0 \tag{4}$$

Momentum conservation:
$$\rho_0 \frac{\partial \mathbf{v}}{\partial t} + \rho_0 \, \mathbf{v} \cdot \nabla \left(\frac{\mathbf{v}}{g_l} \right) = \mu \cdot \nabla^2 \mathbf{v} - g_l \frac{\mu}{K} \mathbf{v} - g_l \nabla p - g_l \rho_0 \left[\beta_T \left(T - T_0\right) + \beta_C \left(C_l - C_0\right) \right] \mathbf{g} \tag{5}$$

The mushy zone is a porous medium saturated with liquid. Its permeability is defined through the Carman-Kozeny relation:
$$K = \frac{\lambda_2^2 g_l^3}{180 \left(1 - g_l\right)^2} . \tag{6}$$

The present work focuses is on the evaluation of the Darcy term (second term on the RHS of equation (5)) using different finite-volume discretization schemes. In the finite volume technique used [8], all scalar variables (enthalpy, temperature, pressure, etc.) are computed at the center of the pressure CVs, while a staggered grid is used to determine the components of the velocity at the faces of the pressure CVs. The SIMPLEC algorithm is used to treat the pressure-velocity coupling. A specific algorithm, detailed in [2], has been implemented in order to resolve the nonlinearity of the transport equations, and in particular the relationship between temperature and enthalpy.

The only significant forces of the momentum balance in the mushy zone are the Darcy drag, the pressure gradient and the buoyancy. This effectively simplifies the momentum equation (5) to
$$\frac{\mu}{K} \mathbf{v} + \rho_0 \left[\beta_T \left(T - T_0\right) + \beta_C \left(C_l - C_0\right) \right] \mathbf{g} + \nabla p \approx 0 . \tag{7}$$

Due to the strong nonlinear dependence of the permeability K on the liquid fraction g_l, the discretization of the Darcy term is critical for the accuracy of the numerical solution of the flow in the mushy zone. To get the discretized form of this term, we have to approximate its integral across the control volume $\int_V \left(\mu / K\right) \mathbf{v} \, dV$. For the horizontal component of the momentum equation this means integration between the faces ‘w’ and ‘e’ of the velocity CV ‘P’, which corresponds to the adjacent pressure points. This gives $\int_w^e \left(\mu / K\right) v_x S_x \, dx$, where S_x is the surface area of the vertical cross section of the

CV. We point out that in all schemes we approximate the velocity to be constant across the whole velocity CV. With constant viscosity the integral is evaluated as

$$\int_w^e \frac{\mu}{K} v_x S_x dx \approx \mu v_{x,P} S_x \int_w^e \frac{dx}{K} \approx \frac{\mu}{\bar{K}_P} v_{x,P} S_x (x_e - x_w) \tag{8}$$

where $\bar{K}_P$ is the effective discretized value of the permeability in the velocity CV 'P', which is evaluated using an approximation of the integral $\int_w^e K^{-1} dx$ by an interpolation of K between the faces 'w' and 'e', where it is known. We now introduce four different discretization schemes for the approximation of this integral using different ways of interpolating K between the two adjacent pressure points.

(a) *Linear interpolation* of the permeability between two adjacent cells.
(b) *Harmonic mean* of the permeability between two adjacent cells.
(c) Volume weighted interpolation of the liquid fraction between two adjacent cells and computation of the permeability with the *interpolated liquid fraction*.
(d) *Analytical integration* of the Darcy term *assuming a linear variation of* g_l between the adjacent pressure points 'w' and 'e'. The dependence of the permeability on the liquid fraction $K(g_l)$ is given by equation (6).

$$\frac{1}{\bar{K}_P} = \frac{1}{(x_e - x_w)} \int_w^e \frac{dx}{K\left(g_l(x)\right)}; \qquad g_l(x) = g_{l,w} + (x - x_w) \frac{(g_{l,e} - g_{l,w})}{(x_e - x_w)} \tag{9}$$

3. Results and discussion

We performed simulations for solidification of a Sn-5 wt %Pb binary alloy in a 2D rectangular cavity (the well-known benchmark experiment by Hebditch and Hunt [9], width: 100 mm; height: 60 mm). The cavity is cooled from the left side (a constant heat transfer coefficient and a constant coolant temperature) and the remaining three sides are thermally insulated. The thermophysical property data, boundary conditions and parameters used in the computations are reported in [4]. For the present alloy the thermal and solutal buoyancy are cooperating as the heavier solute (Pb) is rejected into the liquid upon solidification. This thermosolutal configuration tends to create a downward (counter-clockwise) flow in the melt at the cooled side on account of density variations across the mushy zone.

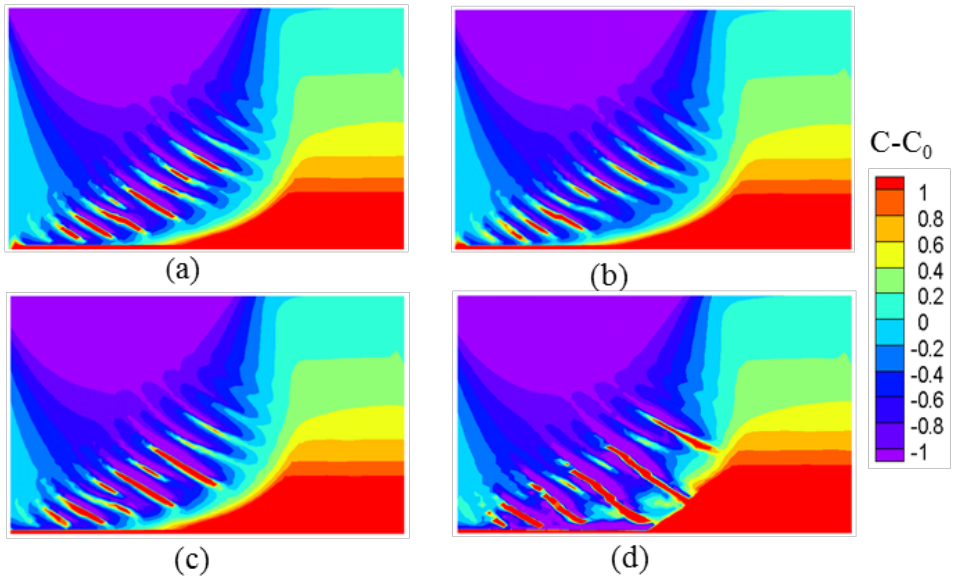


Figure 1. Macrosegregation map at t=400s (60×60 mesh) for different permeability discretization schemes: (a) analytical integration assuming a linear variation of g_l, (b) harmonic mean, (c) interpolated liquid fraction, (d) linear interpolation.

3.1. Macro- and meso-segregation: Effect of discretization schemes

Figure 1 shows segregation maps in the cavity obtained with different discretization schemes and on a regular 60×60 mesh. For all segregation maps (figs. 1a-d) we can see that the flow of solute-rich liquid through the mushy zone towards the bottom of the cavity, driven by the counter-clockwise thermo-solutal convection, results in patches of thin structure in the mushy zone. These patches in the solute field are channel segregates.

A simplified test of the convergence of the permeability discretization schemes was done in our previous paper [4]. We solved the Darcy equation

$$\frac{\mu}{K}\mathbf{v} + \nabla p = 0 \quad . \tag{7}$$

on a specially devised 1D problem, which reproduced solidification conditions (liquid-fraction gradients in the mushy zone) and where a pressure drop was imposed. We compared the velocity predictions of the four discretization schemes to the exact solution of the problem. We clearly showed that all four schemes converge, but the analytical-integration scheme and the harmonic-interpolation scheme give the smallest errors. These two schemes also have opposite signs of discretization error with respect to the calculated velocity; i.e., the analytical-integration scheme tends to overestimate the velocity, while the harmonic-interpolation scheme tends to underestimate the velocity. The linear interpolation scheme gives the largest discretization errors by far and, therefore, needs much denser grids to converge to the other schemes and to the exact solution. This explains the fact that in the full macrosegregation problem the given results are very different from the other schemes on coarse grids (figure 1). In present simulations of the full macrosegregation problem, the results obtained with the linear interpolation scheme (figure 1d) are the farthest from the result obtained using the analytical integration scheme. When using the linear interpolation scheme, one can note that: (1) the number of channels has decreased from 10 to 8, (2) the nature of these channels is completely different compared to the solution using the other three discretization schemes, and (3) the macrosegregation map is also different. Results using the other schemes (analytical integration, interpolated liquid fraction, and harmonic mean) remain in the same range. However, among these three, the analytical integration scheme and the interpolated liquid fraction scheme (figures 1a and 1c) are closer with respect to the predictions of channel segregates. The channel segregates as predicted with the harmonic mean scheme (figure 1b) slightly different and less pronounced.

We found that different discretization schemes give rise to different velocities in the mushy region and hence to a different nature of the segregated channels. For coarser meshes (for example 60×60 nodes) the predictions with the interpolated liquid fraction scheme and the analytical integration scheme are close. However, the prediction with the harmonic mean scheme differs strongly; and the linear interpolation scheme gives completely different results.

3.2. Mesosegregation: effect of mesh size

For 60×60 mesh we saw, that prediction of channel segregates using linear interpolation is far different from the analytical integration and interpolated liquid fraction scheme. For that, the linear interpolation scheme is discarded as inaccurate. Predictions using the interpolated liquid fraction and analytical integration schemes are generally close to each other. The harmonic mean scheme gives slightly different results from the latter two. To study the sensitivity of such differences to the mesh size, we performed simulations with finer meshes for the two most accurate schemes: the analytical integration and the harmonic interpolation scheme. Figure 2 shows that with refinement of grids the difference between the predictions using these two schemes vanishes.

The dependence on mesh size is far greater than that on discretization schemes (for instance see results with 90×90 mesh, 150×150 mesh, and 300×300 mesh in figure 2). Solutions with a very fine mesh show a smaller number of channels, which are all connected to the horizontal channel along the bottom. Furthermore, the inclination and the curvature of the channels are modified, and the there are no channels in the center of the cavity any more. The reason for this reorganization is that the channels are a result of local transport phenomena on a “mesoscopic” scale. These are captured more accurately with finer meshes and the better accuracy appears to have a crucial impact on the predictions.

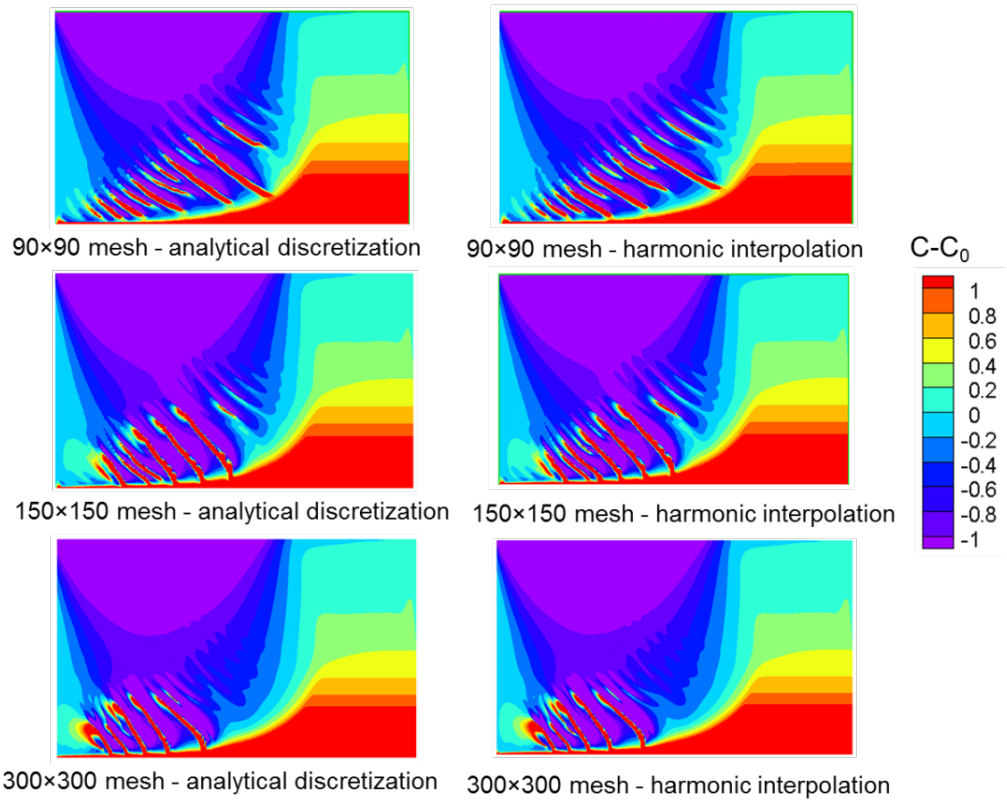


Figure 2. Macrosegregation map at t = 400 s for different mesh size.

Figure 3 shows the flow pattern in the cavity. We can see that the solution on a relatively coarse mesh (90×90) shows a fluid flow that crosses the channels. The solutions on finer meshes (150×150, 300×300, and 500×500) show a flow entering the channels from above and then flowing along the channels. The passage of the flow along the channels is promoted due to their smaller flow resistance. The solute transport in the direction of the flow along the channel causes local enrichment in concentration. This either retards the solidification or induces remelting, and in both cases drives the growth of the channel. As seen in figure 2, the channels merge with finer grids with the horizontal channel at the bottom. This is due to a new organization of local fluid flow with a preferential path along the channel (see figure 3). Because of this reorganization of fluid flow channels from the middle of the cavity disappear, which can be clearly seen in Figure 3 for 300×300 and 500×500 meshes. We also tried to estimate the channel width. For the mesh sizes of 90×90, 150×150, 300×300, and 500×500 the estimated widths are 1685 μm, 1550 μm, 1000 μm, and 980 μm, respectively. The fundamental reason for the reorganization of the flow is that with finer meshes we are starting to resolve the flow in the channel. This of course requires a sufficient mesh resolution. With a channel width of approximately ~1 mm, we can estimate that there are about 1, 1.5, 3, and 5 CVs across a channel, with the meshes that we used (90×90, 150×150, 300×300, and 500×500, respectively). This clearly shows that the coarser grids are insufficient for a solution of the flow in the channels and very fine meshes are absolutely necessary.

We also investigated the evolution of the overall macrosegregation versus the mesh size. We characterize the macrosegregation with the *global segregation index* defined as

$$GSI = \frac{1}{C_0}\left[\frac{1}{V_{\text{domain}}}\iiint_{V_{\text{domain}}}\left(C - C_0\right)^2 dV\right]^{1/2}. \tag{10}$$

The mesh dependence is shown in figure 4. We can see that in the current problem with the coarser meshes, typically with less than 150 nodes (mesh size 0.67 mm) in one direction, the two discretization schemes of the Darcy term give different values for the *GSI*, whereas for finer mesh, the differences vanish.

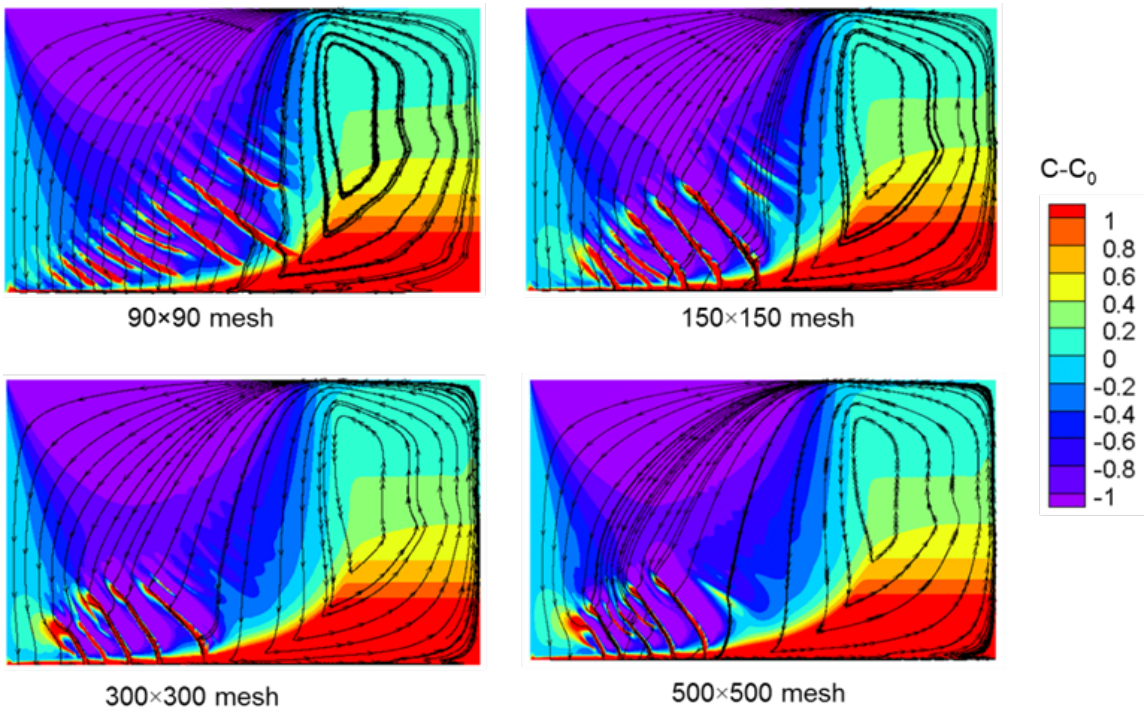


Figure 3. Dependence of the solution on the mesh size: flow field (streamlines) and macrosegregation at 400s for the analytical discretization of permeability.

Moreover, even for the finest mesh 500×500 (mesh size 0.2 mm), the GSI does not reach a stable value that could indicate mesh convergence. Due to prohibitive computational cost we could not check the effect of the further mesh refinement. As noted, we had previously shown the mesh convergence of all four considered scheme on a Darcy test problem [4]. Nevertheless, the solidification problem is more complex and the nonlinearities become stronger than in the Darcy test problem. This should be the reason why we do still not see clear convergence on grids, much finer than those used in the Darcy test problem [4].

For a case of vertical directional solidification, where freckles form, Sung, et al. [10] made a recommendation for proper mesh spacing based on their finite element calculations of directional solidification. They recommended that the element dimensions should be no larger than $2d_1$ in the direction perpendicular to the channel (freckle) axis and no larger than 1.5 D/V in the direction of the channel axis, where d_1 is the primary dendrite arm spacing, D is the diffusivity of the solute in the liquid, and V is velocity of the advancement of the liquid-mushy front. They also suggested that the size of the elements can be made larger than the criteria when it is known *a priori* that the solidification conditions clearly result in freckling or clearly result in non-freckling. We should note that we could not consider such a criterion, since we did not consider macroscopic solute diffusion in the model. In this case the criteria might be more complex. It may also be noted that channeling in the current problem of solidification in a side-cooled cavity is more complex than the vertical unidirectional solidification: there is no zone of stable density gradient in front of the liquidus front and the solute transfer is driven mainly by convection.

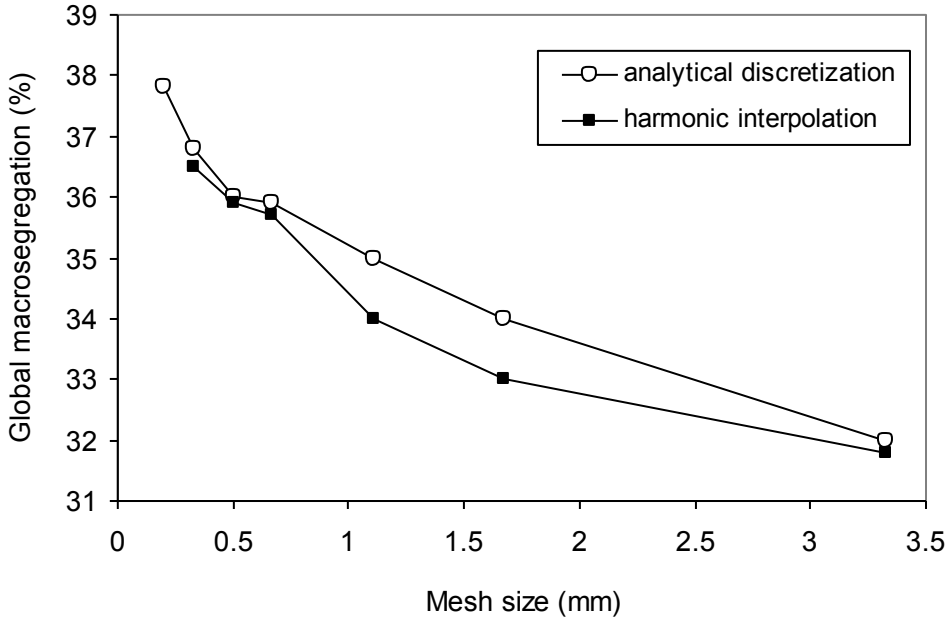


Figure 4. Evolution of the global segregation index versus the number of nodes in one direction.

4. Conclusions

We investigated the dependence of numerical predictions of macro- and mesosegregations on the finite-volume interpolation scheme for the permeability, and on the mesh density. We showed that for simulations with relatively coarse meshes, say for industrial use, the interpolated liquid fraction scheme and the analytical integration scheme are advisable. With finer meshes all discretization schemes give similar results. Sufficient mesh refinement is crucial to capture the complex phenomena occurring in the case of formation of channel segregates. Even in cases where coarse meshes might be able to capture the risk to form channel segregates rather well, only fine meshes are able to resolve the complex phenomena in more detail. With fine meshes, channels we captured channels with several mesh elements across the channel, allowing the estimation of the channel width.

Acknowledgements

This work has been performed in the framework of the project 'SMACS' N°BLAN07-2_193017 financed by the French National Research Agency (ANR).

Nomenclature

Latin Symbols

C	average mass fraction of solute (Pb), wt %
C_0	initial mass fraction of solute (Pb) in the alloy, wt %
c_p	specific heat, J kg^{-1} K^{-1}
g_l	volume fraction of liquid
$\boldsymbol{g}$	gravity vector, m s^{-2}
GSI	global segregation index
h	enthalpy, J kg^{-1}
k	thermal conductivity, W m^{-1} K^{-1}
K	permeability, m^2
L	latent heat of fusion, J kg^{-1}
l	length of the domain, m
p	pressure, Pa
t	time, s
T	temperature, K

$\mathbf{v}$ superficial average velocity, m s^{-1}
$\mathbf{v_l}$ intrinsic velocity of the liquid phase, m s^{-1}
V volume, m^3
V_{domain} volume of the computational domain, m^3

Greek Symbols
β_T thermal expansion coefficient, K^{-1}
β_c solutal expansion coefficient, wt $\%^{-1}$
λ_2 secondary dendrite arm spacing, m
μ dynamic viscosity, kg m^{-1} s^{-1}
ρ mass density, kg m^{-3}

Subscripts
0 reference
l liquid
s solid

References
[1] Prakash C and Voller V R 1989 *Numer. Heat Tr. B–Fund.* **15** 171
[2] Ahmad N, Combeau H, Desbiolles J-L, Jalanti T, Lesoult G, Rappaz J, Rappaz M and Stomp C 1998 *Metall. Mater. Trans. A* **29A** 617
[3] Combeau H, Založnik M, Hans S, and Richy P E 2009 *Metall. Mater. Trans. B* **40B** 289
[4] Kumar A, Dussoubs B, Založnik M and Combeau H 2009 *J. Phys. D: Appl. Phys.* **42** 105503
[5] Založnik M and Combeau H 2010 *Int. J. Therm. Sci.* **49** 1500
[6] Ni J and Beckermann C 1991 *Metall. Mater. Trans. B* **22B** 349
[7] Katz R F and Worster M G 2008 *J. Comput. Phys.* **227** 9823
[8] Patankar S V 1980 *Numerical Heat Transfer and Fluid Flow* (Washington D.C.: Hemisphere)
[9] Hebditch D and Hunt J 1974 *Metall. Trans.* **5** 1557.
[10] Sung P K, Poirier D R and Felicelli S D, 2001 *Int. J. Numer. Meth. Fl.* **35** 357.